

EFFECT OF GAS FLOW RATE ON SEPARATION EFFICIENCY AT DIFFERENT SCALING SCALES OF CYCLONE SEPARATORS

Yangyang Tian^a, Zhuo Chen^{b,*}, Qi Zhuang^c

^a College of Petroleum Engineering, Xi'an Shiyou University, Xi'an, 710065, China

^b The Second Oil Production Plant, Sinopec Northwest Oilfield Company, Urumqi, 830016, China

^c The Second Gas Production Plant, PetroChina Changqing Oilfield Company, Xi'an, 710018, China

ABSTRACT

The cyclone separator has remarkable amplification effect, which is an important factor affecting its separation efficiency and pressure drop. The numerical simulation of Stairmand cyclone separators with cylinder diameters of 200, 280, 400, 480 and 600mm after geometric similarity amplification was carried out by ANSYS software. RSM model was used for gas phase and DPM model was used for particle phase. The results show that after the cyclone size is enlarged geometrically, the tangential velocity tends to increase with the increase of the cyclone barrel diameter at the same inlet gas velocity, which leads to the increase of turbulence energy in the internal flow field of the large size cyclone and the formation of local "eccentric circulation" in the cone section, and causes This leads to an increase in the tangential velocity, which leads to an increase in the turbulent energy in the internal flow field of the large-size cyclone, resulting in the formation of an eccentric ring flow in the cone section, and a tendency for "return flow" and "short-circuit flow" at the lower end of the overflow pipe. The numerical simulation of the particle motion and the experimental results of the separation efficiency both show that the separation efficiency of the Stairmand cyclone for particles of the same size decreases with the enlargement of the barrel diameter; the enlargement effect of the cyclone has little effect on the separation efficiency of particles above 10 μ m in diameter and a significant effect on the separation efficiency of particles below 10 μ m in diameter.

Keywords: Cyclone separator, Size scaling, Numerical simulation, Separation efficiency

1.INTRODUCTION

Cyclone separator has the advantages of simple structure, convenient maintenance and low cost, which is often used in petrochemical, sand and dust removal and other engineering fields. It is a kind of gas-solid separation equipment with high separation efficiency, which can work stably for a long time under complex industrial conditions such as high pressure, high sand content and high temperature (Rietema *et al.*, 1961). Separation efficiency is an important index to evaluate the performance of cyclone separator. At present, theoretical and semi-empirical models, and Computational Fluid Dynamics (CFD) model methods are often used to calculate the separation efficiency of cyclone separators. The main theoretical and semi-empirical models are: equilibrium orbit model, residence time model, bottom flow congestion theory and random orbit theory (Elsayed *et al.*, 2011). The equilibrium orbit model was proposed by Driessen in 1951. It is considered that when the centrifugal force and airflow resistance of the particles in the internal flow field of the cyclone are balanced, the particles outside the equilibrium orbit are spun out by the bottom flow pipe, the particles inside the equilibrium orbit escape from the overflow pipe, and the particles on the separation surface of the equilibrium orbit are discharged by the bottom flow pipe or the overflow pipe with equal probability. The residence time theory was proposed by Rietema in 1961 (Rietema *et al.*, 1961), which considers the particle size that can reach the cyclone wall and be separated out of the bottom flow pipe within the effective residence time as the separation particle size, and Leith and Licht proposed a classical residence time model that considers the interaction between the whole particle group (Leith and Licht., 1972). The bottom flow crowding theory was proposed by Fahlstrom in 1960. In 1981, Dietz *et al.* (1981) proposed a hybrid model

integrating equilibrium orbit theory and residence time model. The theoretical and semi-empirical model of the cyclone separator introduced above requires several ideal assumptions when performing the separation size calculation: (1) the particles are rationalized as spherical; (2) the gravity on the particles is neglected; (3) the gas-solid two-phase density is neglected when it is large.

With the development of Computational Fluid Dynamics (CFD), scholars began to use CFD numerical simulation to study the internal flow pattern of cyclone separator and the influence of variable parameters on its separation performance, and obtained simulation results close to the experimental results. Raoufi *et al.* (2009) used the Reynolds stress turbulence model to calculate the internal flow pattern of cyclone separators and compared it with experimental data. Shukla *et al.* (2013) simulated the two-phase non-constant flow inside the Stairmand high-efficiency cyclone separator using the RSM model and the LES method and predicted the effect of pulsation velocity on the separation efficiency of the cyclone separator. Li *et al.* (2021) used CFD-DPM numerical simulation to trace the trajectory of solid phase particles inside the cyclone and investigated the effect of different particle sizes and inlet gas flow rates on the trajectory of particles inside the cyclone. Jiang *et al.* (2017) established the G-LISR gas-liquid two-phase turbulence model based on the Euler-Lagrange method, and calculated the distribution law of the flow field in the separator at different inlet flow rates using CFD numerical solution.

Entering the 21st century, with the expansion of equipment scale and the increase of sand-containing gases, higher requirements are put forward for the separation performance of cyclone separator. Small size cyclone separators are usually used in laboratory to analyze the separation efficiency of cyclone separators, but in industrial applications,

* Corresponding Author. E-mail: 18691298736@163.com.

large size cyclone separators are usually used for gas-solid separation, and the separation efficiency of cyclone separators with increased size is rarely studied. Therefore, it is of great theoretical importance and engineering value to study the size enlargement effect of cyclones. Jin *et al.* (1990) conducted similar amplification tests with cyclone separators as the base cyclone separator and studied the effect of cylinder diameter amplification on the separation efficiency of cyclone separators. Shao *et al.* (1996) conducted a theoretical study on the amplification effect of cyclone separators based on the basic equations of particle motion. Through numerical simulations, jin *et al.* (2006) found that the pressure drop of the cyclone remained almost constant and the separation efficiency increased when the other dimensions were kept constant and only the diameter of the barrel was increased. Yuan *et al.* (2010) studied that when the inlet gas velocity was certain, the pressure drop of the Stairmand cyclone increased with the increase of the barrel diameter. Yuan *et al.* (2017) conducted experimental studies on Stairmand cyclones with different barrel diameters, and found that when the inlet gas velocity is the same, the increase of bobbin diameter leads to the decrease of separation efficiency and the increase of pressure drop. Existing studies only qualitatively analyze the influence of diameter on the pressure drop and separation efficiency of cyclone separator, but lack of in-depth analysis of the mechanism behind the significant amplification effect of cyclone separator.

In order to solve the above problems, CFD simulation is used to study the flow field change of cyclone separator under scaling effect, and discrete phase model is used to solve the separation efficiency of cyclone separator under scaling effect, which provides a a feasible numerical simulation study for the application of the experimental results of the small-sized laboratory prototype of the cyclone separator to the industrial field. It provides scientific reference and theoretical basis for industrial optimization design of cyclone separator.

2. Geometric Models

This paper takes Stairmand high efficiency cyclone separator as the object of study, selects the optimal experimental model size established by Stefan Obermair as the original size, and uses SolidWorks software to establish the physical model of the cyclone separator, which is shown in Figure 1, the basic structure consists of inlet, cylinder section, cone section, overflow pipe section and bottom flow pipe section (Obermair *et al.*, 2003).

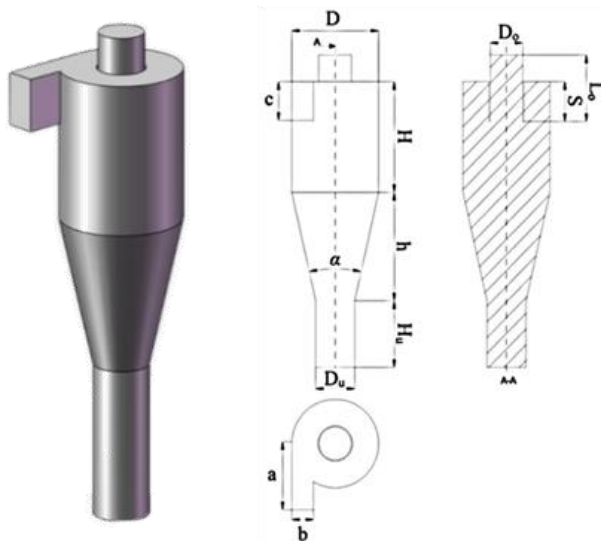


Fig. 1 Geometric model of cyclone separator

In this paper, Stefan Obermair cyclone separator Geo.C-500 structural parameters dimensions are selected as shown in Table 1 (Obermair *et al.*, 2003).

Table 1 Geometric parameters of cyclone separator size table

No.	Parameter name	Symbol	Dimension (mm)
1	Overflow pipe diameter	D _o	150
2	Overflow pipe length	L _o	300
3	Overflow pipe insertion depth	S	180
4	Height of cylindrical section	H	500
5	Diameter of cylindrical section	D	400
6	Height of cone section	h	490
7	Cone angle	α	25.4°
8	Bottom flow pipe height	H _u	500
9	Underflow pipe diameter	D _u	180
10	Inlet length	a	300
11	Inlet width	b	100
12	Inlet height	c	175

3. Calculated solution method

3.1 Turbulence model

Because the internal flow field of cyclone separator is strongly rotating turbulence, it is necessary to select more accurate turbulence model for numerical simulation of its internal flow. At present, the most widely used models are standard k-ε model, RNG k-ε model and Reynolds stress model (RSM). RSM model constitutes a closed N-S equation in three-dimensional flow, which can more accurately simulate the strong cyclone flow in the internal flow field of cyclone separator. Therefore, RSM turbulence model is selected for numerical simulation of turbulence model in this paper.

3.2 Set up the solution control parameters

Because the numerical results depend largely on the selection of control parameters, the following settings are considered in this paper: the solver is selected based on the pressure basis solution method, and the SIMPLEC algorithm with faster convergence is used for the pressure-velocity coupling; because of the rapid pressure changes in the internal flow field of the cyclone separator, the pressure difference complementary format is selected from PRESTO!; the momentum equation, turbulent kinetic energy k, and dissipation rate ε are in the second order upwind format with high accuracy; the Reynolds stress term is adopted in the first-order windward format which is easier to converge, and the steady-state simulation is used to judge its convergence in 5000 iterative steps.

3.3 Numerical simulation study methods for solid particles

In the study of gas-solid two-phase simulation of cyclone separator, it is necessary to adopt appropriate simulation methods. The discrete-phase model is very suitable for the simulation of solid particles with low concentration and small particle size of sand particles. Because the concentration of the particle phase studied in this paper is less than 10%, the collision effect between particles can be ignored in the control equation and momentum equation.

The equation of motion of the particle in the Lagrangian coordinate system is derived from the condition of equilibrium of the forces on the solid-phase particles.

$$\frac{du_p}{dt} = F_D(u - u_p) + g_x(\rho_p - \rho) / \rho_p + F_x \quad (1)$$

$$\begin{cases} F_D = \frac{18\mu}{\rho_p D_p^2} \frac{C_D \text{Re}}{24} \\ \text{Re} = \frac{\rho D_p |u_p - u|}{\mu} \\ C_D = \alpha_1 + \frac{\alpha_2}{\text{Re}} + \frac{\alpha_3}{\text{Re}^2} \end{cases} \quad (2)$$

Where, u_p is the solid particle flow velocity; u is the continuous-phase fluid velocity; ρ , ρ_p is the density of the continuous phase, solid particles; D_p is the particle diameter; g_x is the acceleration of gravity in the x-direction; μ is the coefficient of viscosity; F_x is the external force acting in the x-direction, such as mass force, thermophoretic force; Re is the Reynolds number; C_D is the drag coefficient, α_1 , α_2 , α_3 are constants, given according to the results obtained from the smooth spherical particle experiments.

By solving and calculating the above differential equations, the discrete phase particle motion trajectory can be derived.

3.4 Material media and boundary conditions

The following idealization assumptions are required to solve for the gas-phase flow field inside the cyclone separator. (1) The gas-phase flow inside the cyclone is idealized to be steady-state flow; (2) The gas-phase flow rate at the inlet is idealized to be uniform, ensuring that the internal flow field remains fully developed and turbulent; (3) the gas phase inside the cyclone separator idealized as an incompressible fluid; (4) The temperature of the internal flow field of the cyclone separator is kept constant.

In this paper, for the numerical simulation, the gas-phase medium is selected as air at room temperature and pressure, with a gas-phase density of 1.225 kg/m^3 and a viscosity of $1.7894 \times 10^{-5} \text{ Pa}\cdot\text{s}$. The gas-phase takes a constant velocity into the cyclone, the boundary condition is set to Velocity-Inlet, and the processing gas volume is set to $800 \text{ m}^3/\text{h}$ (12.7 m/s) (Obermair *et al.*, 2003). The turbulence designation method at the gas phase inlet selects the turbulence intensity and the hydraulic diameter. After calculation, $Re=1.10417 \times 10^5$; $I=3.74\%$; $D_H=0.127\text{m}$.

In this paper, the numerical simulation of the gas outlet boundary settings are: the upper overflow port is set to free outflow; the lower bottom flow port is also set to free outflow, the flow weight is set to 1, and the outlet pressure is 1 atm. other boundary conditions are set to wall: the standard wall function is used, considering that the cyclone separator wall is stationary, so the wall is treated as no-slip boundary condition.

In the simulation method of gas-solid two-phase separation, the discrete phase model (DPM) is selected, and the solid particles used in the numerical simulation are 2770 kg/m^3 sand and ash particles with an inlet jet flow rate of 1 g/s . The particles are specified to enter the cyclone with the inlet at the same velocity as the gas phase, and the state of the sand and ash particles are set to spherical, and the particles are set to completely elastic collision with the wall. After the cyclone separator internal cyclone separation, from the lower bottom flow port discharge, a small number of particles due to gas movement will be carried out by the air from the upper overflow port discharge. The boundary conditions are set as follows: the upper overflow port is set as escape, the lower bottom flow port is set as trap, and the wall surface is set as reflect. In this simulation, the inlet particles obey the Rosin-Rammler function distribution, which is very accurate when used to describe the volume distribution of many kinds of materials. The particle distribution function $G(d)$ curve is shown in Figure 2, the minimum particle diameter of $1 \mu\text{m}$, the maximum particle diameter of $10 \mu\text{m}$, the number of particle size is 10. After calculation, the propagation coefficient is 2.48, the median diameter of $4.28 \mu\text{m}$. the cumulative distribution of its particle size is expressed as follows.

$$G(d) = 1 - \exp\left[-\left(\frac{d}{4.28}\right)^{2.48}\right] \quad (3)$$

Where, $G(d)$ is the cumulative distribution function of particle size; d is the particle size.

3.5 Grid delineation and irrelevance verification

The Meshing software in ANSYS is used to divide the hexahedral mesh of the physical model of cyclone separator, as shown in Figure 3. The grid has high precision and good quality, which makes the generated grid closer to the geometric characteristics of cyclone separator, and the grid can be adjusted locally to ensure the accuracy of calculation results; the

inlet and the cylindrical section where the simulation data vary greatly are encrypted to ensure that they have an adequate number of meshes.

The pressure drop and separation efficiency of the cyclone separator are used as reference values to verify the grid irrelevance. As shown in Figure 4, the separation efficiency and the pressure drop of the grid in the process of increasing the number of grids from 180,000 to 850,000 are generally consistent, and the maximum error of the separation efficiency is controlled at 4.6%, and the error of the pressure drop is controlled at about 5.3%. When the number of divided grids is controlled at about 640,000, the separation efficiency and pressure drop no longer change significantly, so the grid number of 640,000 is selected for numerical simulation.

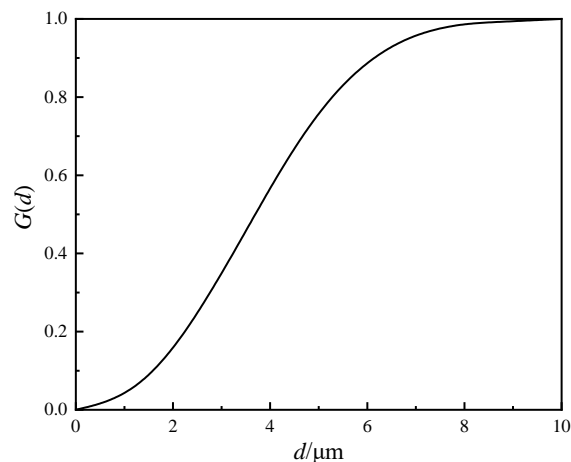


Fig. 2 Particle accumulation distribution function curve

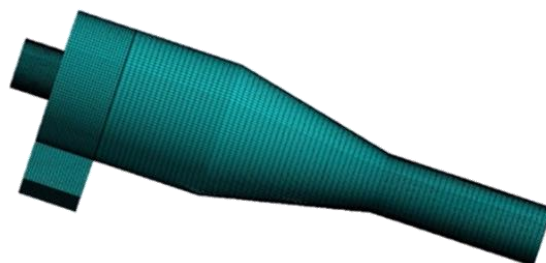


Fig. 3 Meshing of cyclone separator model

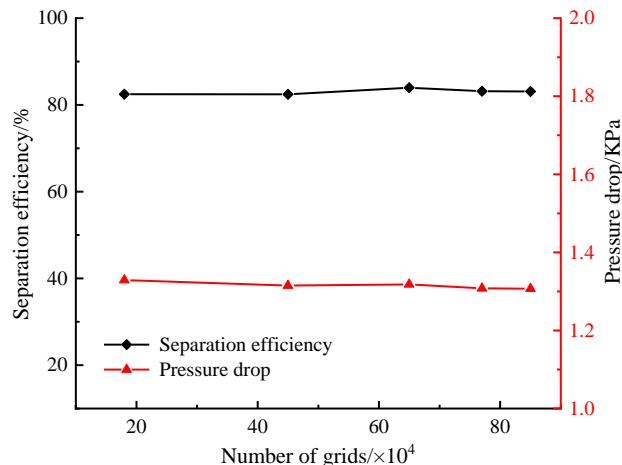
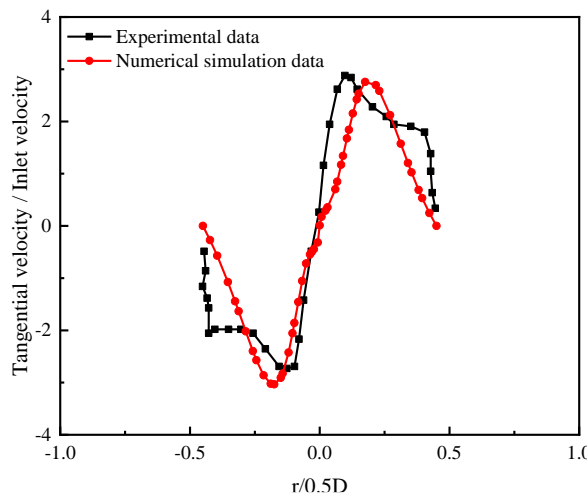
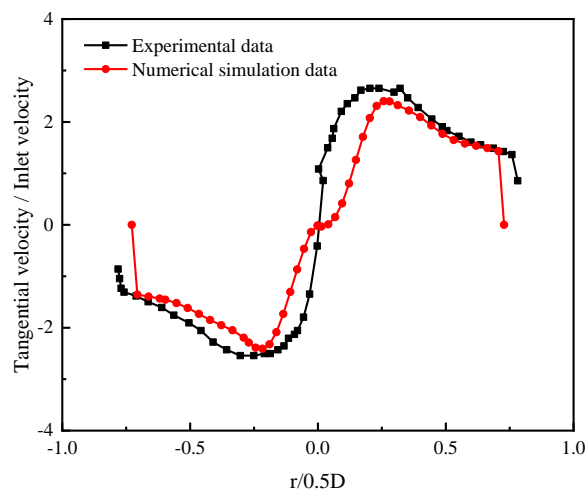
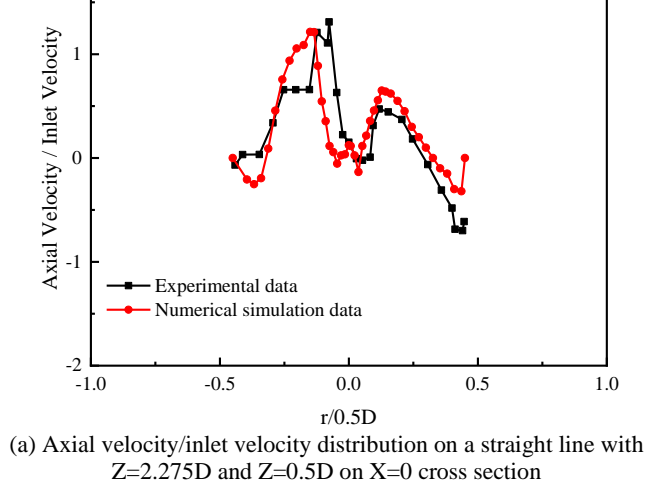
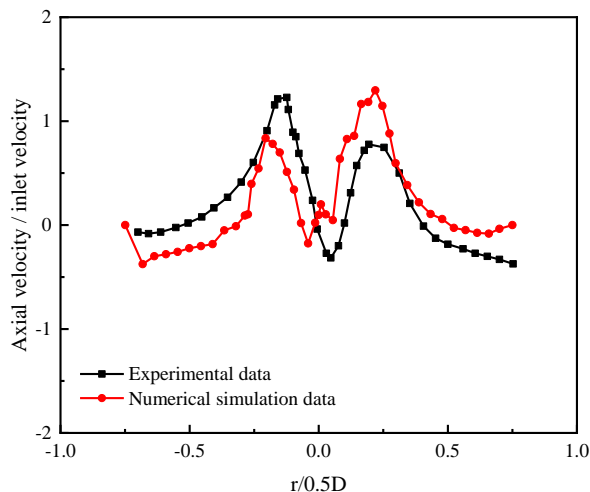


Fig. 4 Model grid-independence verification

3.6 Model accuracy validation

To verify the accuracy of the numerical simulation method in this paper, the selected solution simulation method in this paper was used to compare with the experimental model data of the cyclone separator built by Stefan Obermair. Considering that the experimental data built by Stefan Obermair were obtained at 293.15 K, an outlet pressure of 1 atm, an inlet air volume of 800 m³/h (inlet velocity of 12.7 m/s), and a tracer particle injection rate of 50-100 mg/h, the numerical simulation parameters set in this paper were highly consistent with the experimental conditions, and the data sources were chosen from the literature and the literature (Obermair *et al.*, 2003). The data sources are selected from the literature for comparison with the simulation results under the boundary conditions set in this paper.

As shown in Figure 5, Figure 5(a) shows the comparison between numerical simulation axial velocity/inlet velocity and experimental measurement axial velocity/inlet velocity, it can be seen that the distribution trend of numerical simulation data and experimental measurement data is basically the same; Figure 5(b) shows the tangential velocity/inlet velocity of numerical simulation and experimental data tangential velocity/inlet velocity for radial position dimensionless processing, from the figure it can be seen that the tangential velocity along the radial position is "Rankin combined vortex distribution", that is, the external is quasi-free vortex, the internal is quasi-forced vortex; the degree of agreement with the experimental data is good, and the average error is controlled within 10%, for industrial applications, the numerical simulation method selected in this paper has a high reliability and accuracy.



(b) Tangential velocity/inlet velocity distribution on a straight line with $Z=2.275D$ and $Z=0.5D$ on $X=0$ cross section

Fig. 5 Numerical simulation results of the Reynolds stress model solved for the cyclone compared with experimental measurements (bottom of the cyclone is the zero point, upwards is positive, $D=400\text{mm}$)

3.7 Numerical simulation and experimental measurement data error analysis

From the above numerical simulation and experimental measurement data comparison, it can be seen that the numerical simulation results and experimental results of the general trend towards a good degree of agreement, but there are still certain errors. Comparing the experimental data with the numerical simulation data, and combining with the research status of cyclone separators at home and abroad, several possible reasons for the errors between them are put forward.

(1) Laser Doppler Anemometry (LDA) system errors have been well controlled through years of research, and the cause of the errors may be due to droplet slip, which is generated by the difference between the velocity of the gas phase and the velocity of the tracer droplet. Because of the complex flow field inside the cyclone and the large centrifugal force, the tracer droplet velocity may track slowly and deviate from the actual gas phase velocity, so the numerical simulation and the experimental data produce errors.

(2) The LDA probe is not aligned with the central axis of the cyclone, because there is a deviation between the cyclone axis and the axis of the measuring instrument, which means that the coordinate system will produce a certain error, affecting the tangential velocity, axial velocity and radial velocity values, in the data analysis, it is necessary to use the "Dwell time" weights are used to correct the data for velocity errors.

In summary, the numerical simulation using the selected solution algorithm and boundary conditions is very consistent with the experimental model developed by Stefan Obermair, which can be used to support the reliability of subsequent research.

4. Effect of flow field variation inside cyclone separators on separation efficiency at different scaling scales

4.1 Geometric modeling of cyclone separators at different scaling scales

The cyclone structure is scaled to different degrees, and the parameters are reduced or enlarged in full size on the basis of the original size cylinder section diameter D . Four model sizes are designed for 0.5D, 0.7D, 1.2D and 1.5D respectively (the bottom of the cyclone is the zero point and upwards is positive).

The gas inlet velocity (set three velocities 10m/s, 12.7m/s, 15m/s) is changed to study the separation efficiency of the cyclone separator under different scaling sizes, and the effect of velocity change on the separation efficiency of the cyclone separator under different scaling scales is analyzed by the change of tangential velocity flow field in different geometric models.

4.2 Analysis of tangential velocity flow field of cyclone separator under different scaling scales

The tangential velocities at four positions of $Z=0.75D$, $Z=1.5D$, $Z=2.25D$ and $Z=3.0D$ on $X=0$ cross-section was analyzed to determine the internal flow field variation of the cyclone separator. Figure 6 gives the tangential velocity comparison clouds of the internal flow field of the cyclone separator at the inlet velocity of 10m/s for five structural dimensions $X=0$ cross-section, where the radial $Z=3.0D$ cross-section is intercepted for comparison.

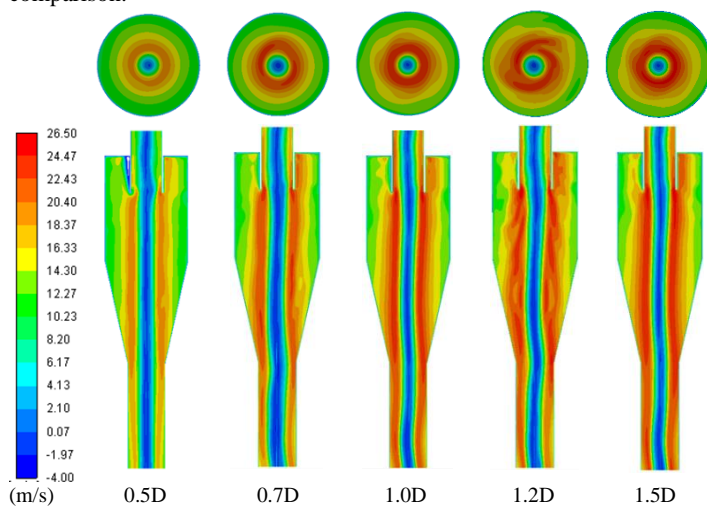


Fig. 6 Tangential velocity cloud of cyclone separator inlet velocity at 10m/s at different scaling scales

Figure 7 gives the tangential velocity comparison clouds of the internal flow field of the cyclone separator at the inlet velocity of 12.7m/s for five structural dimensions $X=0$ cross-section, where the radial $Z=3.0D$ cross-section is intercepted for comparison.

Figure 8 gives the tangential velocity comparison clouds of the internal flow field of the cyclone separator at the inlet velocity of 15m/s for five structural dimensions $X=0$ cross-section, where the radial $Z=3.0D$ cross-section is intercepted for comparison.

As can be seen from Figure 6,7,8, the intercepted cross sections of the cyclone separator under five scaling scales are equated in the paper, and the tangential velocity distribution along the Z -axis (zero point at the bottom of the cyclone separator and positive upward) shows a trend of continuously getting larger as the inlet velocity increases, and the tangential velocity in the cylindrical section is obviously higher than the

velocity in the bottom flow section, which indicates that the cyclonic strength in the cylindrical section of the cyclone separator is stronger than that in the bottom flow section; Figure 6,7,8 also shows that the tangential velocity of 0.5D and 0.7D reduced size changes more obviously, and the overall tangential velocity shows a decreasing law, when the original size is enlarged, the incremental value of tangential velocity under 1.2D and 1.5D size does not change much, but the overall law shows the law of increasing from small to large, which is caused by the small size selected for enlargement. Overall, the overall tangential velocity distribution is in good agreement with the experimental data, showing a "Rankine" vortex structure distribution. It can be seen that the closer the cylinder section is to the cyclone wall, the weaker the ability of the gas to carry the particles, reducing the kinetic energy of the solid phase particles, which is conducive to the particles being settled to the bottom flow port under the action of gravity. In the bottom flow section, the velocity reduction trend of the quasi-forced vortex outside the separator near the wall is not as fast as that of the cylindrical section, which is caused by the sharp decrease in the axial diameter of the cyclone in the cone section.

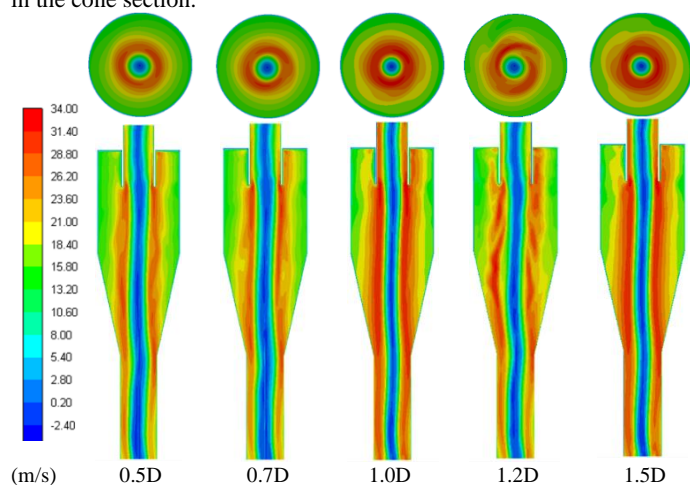


Fig. 7 Tangential velocity cloud of cyclone separator inlet velocity at 12.7m/s at different scaling scales

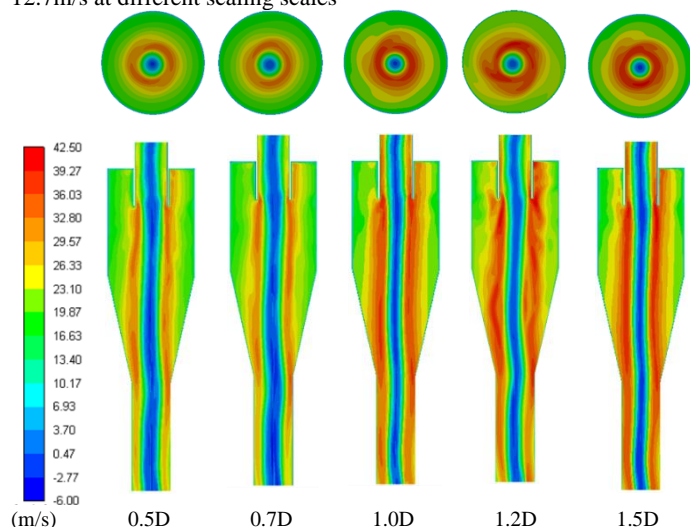


Fig. 8 Tangential velocity cloud of cyclone separator inlet velocity at 15m/s at different scaling scales

4.3 Study of secondary flow in the velocity flow field of a cyclone separator

The flow field inside the cyclone separator is complex, and the internal flow field movement law is mainly determined by the tangential velocity, axial velocity and radial velocity together. In addition, due to the combined effect of axial and radial velocities in the cyclone separator

flow field, a secondary flow inside the flow field is generated, which is not conducive to particle removal in the cyclone separator and affects its separation performance. Therefore, the study of the secondary flow is of theoretical importance to improve the separation performance of the cyclone separator(Wang, 2020).

The cyclone separator is divided into the following categories according to the location where the secondary flow occurs as shown in Figure 9: longitudinal circulation in the annular space of the top plate, short-circuit flow at the lower end of the overflow pipe, eccentric circulation at the lower end of the cone section and re-mixing flow at the lower end of the bottom flow section.

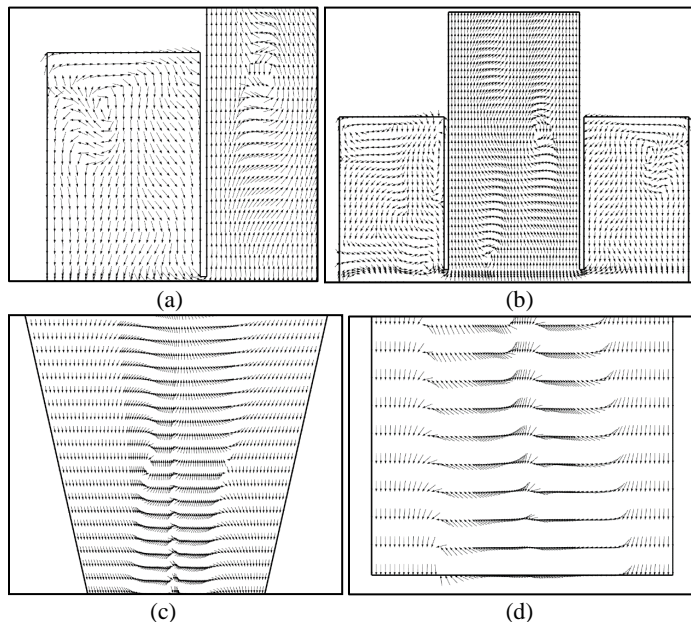


Fig. 9 Distribution of the four types of secondary flow in the cyclone separator

As shown in Figure 9(a), the formation of longitudinal circulation is mainly due to the existence of a slow flowing boundary layer in the annular space under the top plate of the cyclone, so the fluid with high static pressure at the outer wall can easily flow into this boundary layer and move towards the radial inner side of the cyclone, forming a circulation. The longitudinal circulation will carry a small number of particles that have been separated to the outer wall of the cylinder upwards and remain in the annular space under the top plate, resulting in the phenomenon of "top ash ring", thus reducing the separation efficiency of the cyclone separator.

As shown in Figure 9(b), the short-circuit flow is formed by the existence of a secondary flow from its inner wall surface to the outer wall of the overflow tube in the annular space under the cyclone's top plate. The short-circuit flow carries the unseparated particles along the overflow opening and is blown directly out of the cyclone, which can greatly reduce the separation efficiency of the cyclone, and the single particle short-circuit flow trajectory is shown in Figure 10.

As shown in Figure 9(c), an eccentric longitudinal circulation exists at the lower end of the cone section of the cyclone separator. Tan et al. (1984) suggest that the eccentric circulation is generated because at the lower end of the cone section as the radius of external rotation of the outer vortex airflow decreases sharply, the downward airflow near the outer wall surface of the separator will intersect and collide with the rising airflow in the axial inner vortex, resulting in strong momentum exchange and turbulent dissipation, forming an eccentric circulation.

As shown in Figure 9(d), the formation of re-mixing flow is due to a sharp increase in the tangential velocity of the airflow movement due to a sharp decrease in the radius of rotation of the outer vortex fluid, which eventually forms a negative pressure zone near the bottom flow opening that is lower than the pressure in the outer space, resulting in the

possibility of the outer space fluid entraining the separated particles into the negative pressure zone and being carried into the separator again with the airflow movement in the negative pressure zone, forming a re-mixing flow.



Fig. 10 Schematic diagram of a single particle simulating short-circuit flow operation

4.4 Effect of different gas flow rates on pressure drop in cyclone separators with different scaling sizes

Pressure drop is an important indicator of the separation performance of the cyclone separator, scholars have done in-depth research on the separation performance of the cyclone separator and pressure drop, it is generally believed that the smaller the pressure drop, the smaller the internal energy loss of the cyclone separator, the relationship between separation efficiency and pressure drop is often contradictory, the increase in separation efficiency is often accompanied by an increase in pressure drop. Figure 11 gives the pressure drop values for the five scaled cyclone sizes for six sets of inlet velocities(10m/s, 12.7m/s, 15m/s, 20m/s, 25m/s, 30m/s)

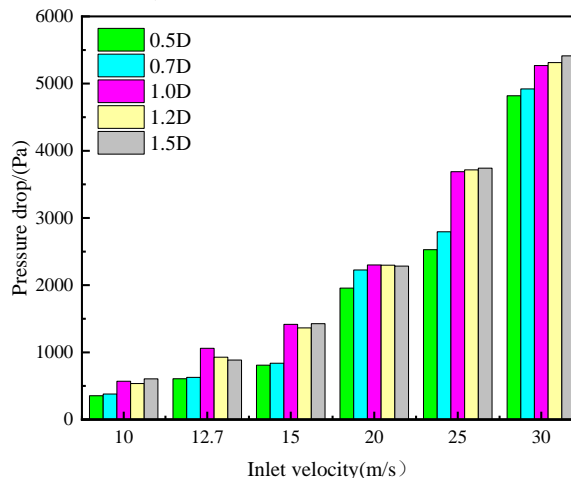


Fig. 11 Effect of cyclone scaling size on pressure drop at different inlet velocity

The comparison shows that the pressure drop tends to increase with larger cylinder diameter for the same inlet velocity, but the effect is not obvious. For the same structure, the larger the inlet velocity, the larger the pressure drop, and the effect is very obvious. The pressure drop at a velocity of 30 m/s is nearly 2.5 times higher than that at 20 m/s. This is due to the fact that the higher the inlet velocity, the higher the rotational intensity of the gas flow, resulting in a lower central static pressure. As the gas enters the bottom and overflow pipe, the dynamic pressure increases according to the law of conservation of angular momentum because of the small diameter of this pipe. The energy of dynamic pressure is dissipated in the overflow pipe and bottom flow pipe, resulting in the increase of pressure drop loss.

In short, increasing the inlet velocity will increase the pressure drop, but from the point of view of energy consumption, excessive flow will lead to serious wear on the inner wall of cyclone separator, which will affect the service life of cyclone separator, because the wear on the inner wall is proportional to the fourth power of gas flow. This is particularly important.

4.5 Effect of inlet velocity on classification efficiency of cyclone separators with different scaling sizes

In order to verify the accuracy of using the discrete phase model, the results of the cyclone variation with particle size were simulated using an inlet air volume of 800 m³/h (inlet velocity 12.7 m/s) and compared with the experimental results under the same conditions established by Stefan Obermair, as shown in Figure 13(Obermair *et al.*, 2003).

From Figure 12, it can be seen that the simulation results obtained by CFD-DPM method have some error with the experimental results. This error is due to the deviation of the RSM turbulence model describing the turbulence action of the airflow from the actual turbulence action of the internal flow field of the cyclone separator. Overall, the use of CFD-DPM model can better reflect the separation performance of the cyclone separator.

Based on the verification of the reliability of the CFD-DPM model, the effect of four sets of inlet velocity variations (15m/s, 20m/s, 25m/s,

30m/s) on the classification efficiency of the cyclone at the scaling scale was simulated and calculated, and the relationship between the inlet velocity and the classification efficiency is shown in Figure 13

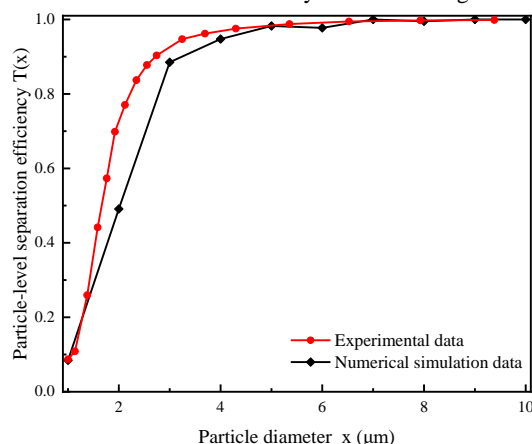
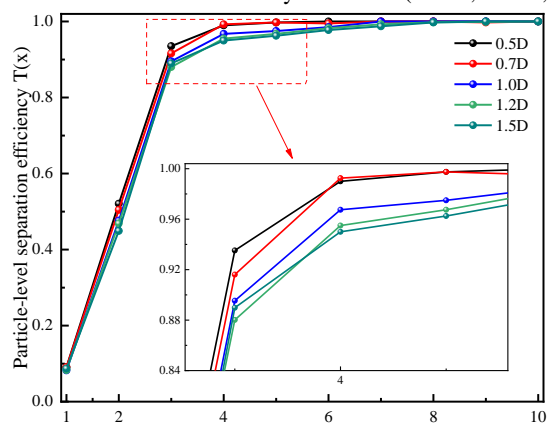
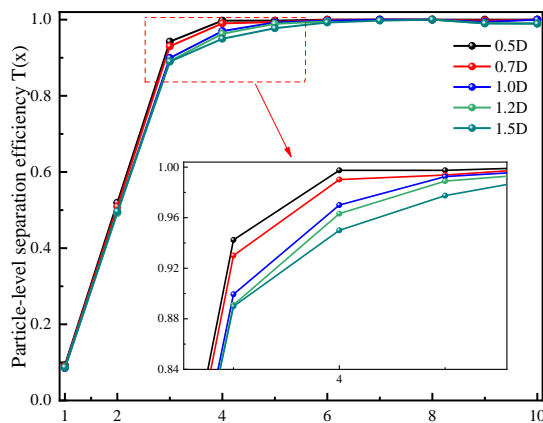


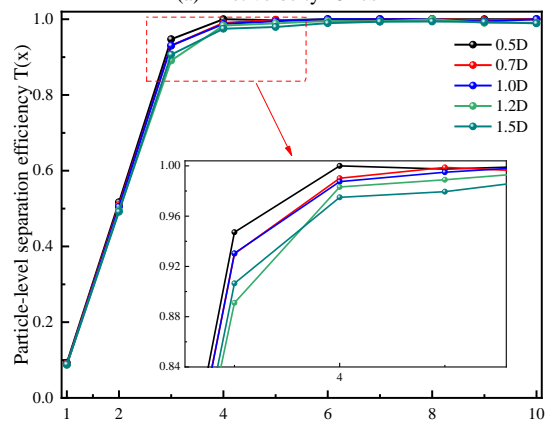
Fig. 12 Comparison between numerical simulation results and experimental results of classification efficiency at inlet Velocity of 12.7m/s



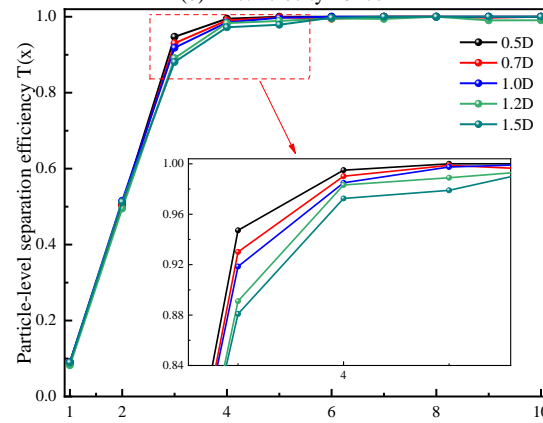
(a) Inlet velocity 15m/s



(b) Inlet velocity 20m/s



(c) Inlet velocity 25m/s



(d) Inlet velocity 30m/s

Fig. 13 Effect of cyclone separators scaling size on classification efficiency at different inlet velocities

Figure 13 shows that as the particle diameter increases, the classification efficiency of the cyclone separators under the five scaled sizes also increases; for fine particles, the separation effect of the cyclone separator under the 0.5D reduced size is better than that of the cyclone separator under the 1.5D enlarged size, and for particles above 10μm, the cyclone separators under the five scaled sizes can completely separate them. In conclusion, it can be seen that the separation effect of the

cyclone separator for fine particles decreases significantly with the scaled-up size of the cyclone separator.

With the increasing inlet flow velocity, the separation efficiency of the cyclone separator under five groups of scaling scales obviously shows an increasing trend, but it does not mean that the velocity can be increased all the time. From the comparison of Figure 13(c) and (d), the separation efficiency under 30m/s inlet velocity, compared with the

separation efficiency under 25m/s inlet velocity, shows a decrease. Combined with the tangential velocity distribution, with the enlargement of the cyclone size, the tangential velocity value shows a tendency to increase. The increase of the tangential velocity can make the internal flow field of the cyclone fully developed, and it is easier to recoil the separated fine particles, which causes serious back-mixing flow and reduces the separation efficiency of the cyclone separator.

Separation efficiency as an important criterion to measure the cyclone separator, the total separation efficiency of the cyclone separator is investigated in this paper based on the analysis of the particle-level separation efficiency. The separation efficiencies of cyclone separator with different scaling scales for different inlet velocities are given in Figure 14.

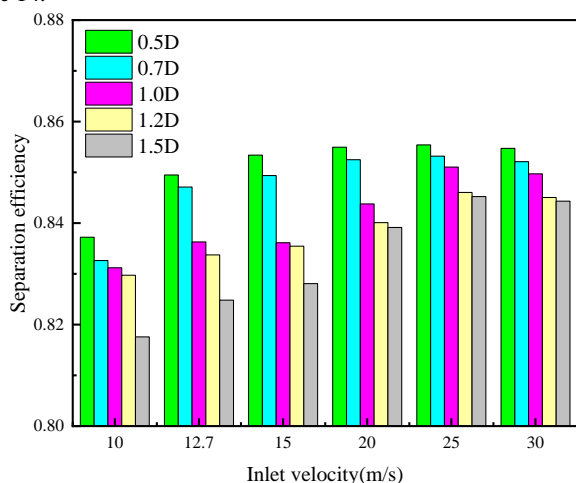


Fig. 14 Separation efficiency of the scaling size cyclone separators at different inlet velocities

From Figure 14, it can be seen that the separation efficiency increases rapidly when the inlet velocity increases from 10m/s to 20m/s. The separation efficiency tends to rise steadily at 20m/s-25m/s, and decreases slightly in the 25m/s-30m/s velocity section. This law is due to the fact that the increase in inlet velocity leads to more violent collisions between particles, resulting in the increased probability of re-mixing and short-circuiting, which in turn leads to poor separation efficiency of cyclone separators with increased inlet velocity. The wear equation of cyclone separator is proportional to the quadratic inlet velocity, so choosing the right inlet velocity not only ensures its separation efficiency, but also prolongs the service life of cyclone separator. Taken together, the optimal inlet velocity of the cyclone selected in this paper should be kept between a reasonable range of 20m/s-30m/s.

4.6 Technical parameters of the processing capacity of cyclone separator under scaling scale

The classification efficiency of the cyclone separator was studied by changing inlet velocity under scaling size, and the technical parameters of the cyclone separator processing capacity under scaling effect were summarized based on CFD-DPM model, as shown in Table 2.

4.7 Industrial application and experimental validation of cyclone separators

In this study, the scaled-up cyclone separator device is applied to industrialization, and the gas-solid separation operation has been completed on site at a gas field wellhead in China. The device has a maximum operating pressure of 70 MPa, a maximum processing capacity of 100,000 m³/day of gas, and a maximum processing capacity of 2.5 m³/day of sand. From the field application results, the device can achieve complete separation of solid particles above 10μm, and the separation effect for particles above 5μm can reach 70%.

The physical diagram of the device and the sand samples obtained after gas-solid separation are shown in Figure 15 and Figure 16, respectively.

Table 2 Technical parameters of cyclone separator processing capacity at scaling scale

No.	Cylinder diameter /mm	Underflow pipe diameter /mm	Processing Capacity	particle size	Separation efficiency
0.5D	DN200	DN90	157(m ³ /h)	1-10μm	83.7%
			200(m ³ /h)		84.9%
			236(m ³ /h)		85.3%
			315(m ³ /h)		85.4%
			393(m ³ /h)		85.5%
			472(m ³ /h)		85.4%
0.7D	DN280	DN126	308(m ³ /h)	1-10μm	83.2%
			392(m ³ /h)		84.7%
			463(m ³ /h)		84.9%
			617(m ³ /h)		85.2%
			771(m ³ /h)		85.3%
			926(m ³ /h)		85.2%
1.0D	DN400	DN180	630(m ³ /h)	1-10μm	83.1%
			800(m ³ /h)		83.6%
			945(m ³ /h)		83.6%
			1260(m ³ /h)		84.3%
			1575(m ³ /h)		85.1%
			1890(m ³ /h)		84.9%
1.2D	DN480	DN216	907(m ³ /h)	1-10μm	82.9%
			1152(m ³ /h)		83.3%
			1360(m ³ /h)		83.5%
			1814(m ³ /h)		84.0%
			2268(m ³ /h)		84.6%
			2721(m ³ /h)		84.5%
1.5D	DN600	DN270	1417(m ³ /h)	1-10μm	81.7%
			1800(m ³ /h)		82.4%
			2126(m ³ /h)		82.8%
			2835(m ³ /h)		83.9%
			3543(m ³ /h)		84.5%
			4252(m ³ /h)		84.4%



Fig. 15 Diagram of the cyclone device after enlarging the size



Fig. 16 Solid sand particles after cyclone separator separation

Experimental validation was carried out by comparing the numerical simulation results of a Stairmand cyclone with a cylindrical diameter of 600 mm with the experimental results. The separated gaseous sand grains were placed in a Hydro2000MU with water and stirred, followed by particle size measurements using a Malvern Insittec laser particle sizer. The operation is as follows: a. The optical path has to be calibrated before the measurement; b. Using distilled water as the measurement background, 700 ml is taken and poured into the beaker of the Hydro2000MU device, the microwave is turned on for 10 s to remove air bubbles from the distilled water, the stirring pump is turned on and the background was measured; c. The sand mixture to be measured is slowly poured into the beaker of the Hydro2000MU device and the shading rate is observed. Ensure that the shading rate is between 10% and 25%; d. Start the measurement and save the results.

To ensure the accuracy of the measurements, samples were taken three times and added to the beaker of the Hydro2000MU device within 15 s of each sample being taken and stirred. The beaker was washed with distilled water at the end of each measurement, no less than three times, to ensure that no sand remained in the instrument tube or beaker before the next sand sample was measured as described above. The Hydro2000MU and Malvern Insittec laser particle sizing devices are shown in Figure 17.



(a) Hydro2000MU Device



(b) Malvern Insittec Device

Fig. 17 Hydro2000MU with Malvern Insittec Laser Particle Measuring Device

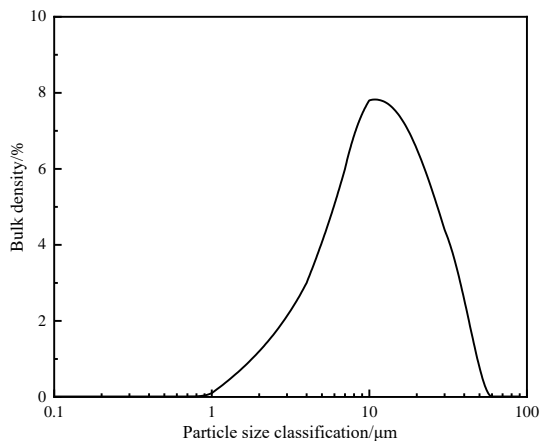


Fig. 18 Distribution of particle size of raw material

Figure 18 shows the particle size distribution of the raw material with an average particle size of 15μm. At an inlet gas velocity of 20m/s, the measured classification efficiency of the Stairmand cyclone was compared with the numerical simulation data as shown in Table 3.

Table 3 Cyclone classification efficiency at an inlet velocity of 20 m/s

No.	Average particle size/μm	Numerical simulation of separation efficiency/%	Experimental of separation efficiency/%	Relative error/%
1	1	8.775	10.10	15.1
2	2	49.640	43.45	12.5
3	3	88.978	84.20	5.36
4	4	95.000	94.50	0.51
5	5	97.750	96.30	1.48
6	6	98.250	97.20	1.06
7	7	98.750	97.45	1.31
8	8	98.890	97.80	1.10
9	9	99.100	98.20	0.91
10	10	99.450	98.90	0.55
11	20	/	99.90	/
12	30	/	99.90	/
13	40	/	99.90	/
14	50	/	99.90	/

As can be seen from Table 3, the numerical simulation of the separation efficiency of the 600 mm diameter cyclone at the same gas velocity is in good agreement with the experimental data; this indicates that the simulation results are accurate and that the increase in the diameter of the cylinder reduces the separation capacity and efficiency of the cyclone.

5. CONCLUSIONS

In this paper, CFD numerical simulation is used to study the separation performance of proportional cyclone separator at different inlet velocities. By analyzing the change of internal flow field, the relationship between separation efficiency and size ratio is obtained.

(1) When the cyclone is scaled at the same inlet velocity, the tangential velocity distribution pattern shows a "Rankine" vortex structure distribution as the cyclone is scaled up in size, and the tangential value tends to increase, which is an important factor for the scaling effect of the cyclone.

(2) After the size of the cyclone separator is enlarged, the internal flow field produces the phenomenon of secondary flow, which is not conducive to the separation of solid particles in the cyclone separator and directly affects the separation efficiency of the cyclone separator.

(3) The results for the separation efficiency of the cyclone at six different inlet velocities for scaled sizes show that keeping the inlet velocity in the range of 20m/s-30m/s ensures efficient separation efficiency and maximises the service life of the cyclone.

(4) The numerical simulation and experimental test results of the classification efficiency of the cyclone separator both show that the separation efficiency of the same particle size decreases with the increase of the cyclone separator barrel diameter. The amplification effect of the cyclone separator reduces the separation efficiency of fine particles below 10 μm more significantly, while the effect on the separation efficiency of particles above 10 μm is not significant. The numerical simulations are in general agreement with the experimental results, with some errors, but the errors are small. The results obtained from the numerical simulations can provide guidance for the design of the cyclone size structure in industry.

ACKNOWLEDGEMENTS

This work is supported by the Scientific Research Program Funded by Shaanxi Provincial Education Department (Program No. 21JK0831), and the Natural Science Basic Research Program of Shaanxi (Program No. 2021JQ-602).

NOMENCLATURE

u_p — solid particle flow velocity, m/s
 u — continuous-phase fluid velocity, m/s
 ρ — density of the continuous-phase, kg/m³
 ρ_p — density of the solid particles, kg/m³
 D_p — particle diameter, m
 g_x — acceleration of gravity in x direction, m/s²
 μ — viscosity coefficient, Pa·s
 F_x — external force acting in the x direction, N

REFERENCE

Chen, L. J., Ma, H., Guan guo Ma, G. G., Li, P. C., Li, C. K., Cong, X. C. (2022). Effect of inlet periodic velocity on the performance of standard cyclone separators. *Powder Technology*, 402, 117347. <https://doi.org/10.1016/j.powtec.2022.117347>.

Chu, K. W., Wang, B., Xu, D.L., and Chen, Y. X. (2021). CFD–DEM simulation of the gas–solid flow in a cyclone separator. *Chemical Engineering Science*, 66(5), 834–847. <https://doi.org/10.1016/j.ces.2010.11.026>.

Dang K. L., Joon Y. Y. (2020). Numerical investigation on the performance and flow pattern of two novel innovative designs of four-inlet cyclone separator. *Chemical Engineering and Processing - Process Intensification*, 150, 107867. <https://doi.org/10.1016/j.cep.2020.107867>.

Dietz, P. W. (1981). Collection efficiency of cyclone separators. *AIChE Journal*, 27(6), 888–892. <https://doi.org/10.1002/aic.69027060>

Eflita, Y., Mohammad, T., Rifky, I., Anggi, M., Henry, C., Farkhan, H. Dwinanda, H. D. A., Mohamad, E. Y., and Kwang-Hwan, C. (2023). The effect of cylinder wall cooling and vortex finder (tapered in-out) geometry on temperature, heat rate, and flow field to increase cyclone performance using CFD. *Case Studies in Chemical and Environmental Engineering*, 7, 100311. <https://doi.org/10.1016/j.cscee.2023.100311>.

Elsayed, K., and Lacor, C. (2011). The effect of cyclone inlet dimensions on the flow pattern and performance. *Applied mathematical modelling*, 35(4), 1952–1968. <https://doi.org/10.1016/j.apm.2010.11.007>

Farzad, P., Seyyed, H. H., Khairy, E., and Goodarz, A. (2018). Numerical investigation of effects of inner cone on flow field, performance and erosion rate of cyclone separators. *Separation and Purification Technology*, 201, 223–237. <https://doi.org/10.1016/j.seppur.2018.03.001>.

Gao, X., Chen, J. F., Feng, J. M., Peng, X. Y. (2014). Numerical investigation of the effects of the central channel on the flow field in an oil–gas cyclone separator. *Computers & Fluids*, 92, 45–55. <https://doi.org/10.1016/j.compfluid.2013.11.001>.

Gao, Z. W., Wang, J., Liu Z. X., Wei Y. D., Wang, J. Y., and Mao, Y. (2020). Effects of different inlet structures on the flow field of cyclone separators. *Powder Technology*, 372, 519–531. <https://doi.org/10.1016/j.powtec.2020.06.014>.

Jang, K., Lee, G. G., & Huh, K. Y. (2018). Evaluation of the turbulence models for gas flow and particle transport in URANS and LES of a cyclone separator. *Computers & Fluids*, 172, 274–283. <https://doi.org/10.1016/j.compfluid.2018.04.032>

Jiang Z. X., Xu L., Xiang D., Yang M., Guo Z. (2017). Effect of different gas phase inlet flow rates on the flow field characteristics of G-LISR. *Chemical Reaction Engineering & Processes*, 33(03), 227–235.

Jin, W., Lee, H. J., Yang, D. Y., (2006) Effect of the cylinder shape of a long-coned cyclone on the stable flow-field establishment. *Powder Technology*, 165(01), 30–38. <https://doi.org/10.1016/j.powtec.2006.03.011>.

Jin, Y., Shi M. X. (1990). Experimental study on similar amplification of cyclone separator. *Journal of Petroleum University (Natural Science Edition)*, 05, 46–55.

Leith, D., and Licht, W. (1972). The Collection Efficiency of Cyclone Type Particle Collectors—A New Theoretical Approach. *In AIChE Symp*, 68(126), 196–206.

Leith, D., and Mehta, D. (1973). Cyclone performance and design. *Atmospheric Environment* (1967), 7(5), 527–549. [https://doi.org/10.1016/0004-6981\(73\)90006-1](https://doi.org/10.1016/0004-6981(73)90006-1)

Li, X. D., Yan, J. H., Cao, Y. C., Ni, M. J., and Cen, K. F. (2003). Numerical simulation of the effects of turbulence intensity and boundary layer on separation efficiency in a cyclone separator. *Chemical Engineering Journal*, 95(1–3), 235–240. [https://doi.org/10.1016/S1385-8947\(03\)00109-8](https://doi.org/10.1016/S1385-8947(03)00109-8).

Lidén, G., and Gudmundsson, A. (1997). Semi-empirical modelling to generalise the dependence of cyclone collection efficiency on operating conditions and cyclone design. *Journal of aerosol science*, 28(5), 853–874. [https://doi.org/10.1016/S0021-8502\(96\)00479-X](https://doi.org/10.1016/S0021-8502(96)00479-X)

Ma, L., Ingham, B. B., Wen, B. (2000). Numerical modelling of the fluid and particle penetration through small sampling cyclones. *Journal of Aerosol Science*, 31(9), 1097–1119. [https://doi.org/10.1016/S0021-8502\(00\)00016-1](https://doi.org/10.1016/S0021-8502(00)00016-1).

Mehdi, M., Hadi, N., Hamed, S. (2021). Modeling and numerical simulation of flow field in three types of standard new design cyclone separators. *Advanced Powder Technology*, 33(11), 4295–4302. <https://doi.org/10.1016/j.appt.2021.09.037>.

Misiulia, D., Antonyuk, S., Andersson, A. G., and Lundström, T. S. (2020). High-efficiency industrial cyclone separator: A CFD study. *Powder Technology*, 364, 943–953. <https://doi.org/10.1016/j.powtec.2019.10.064>

Mothilal, T., Pitchandi, K. (2015). Influence of inlet velocity of air and solid particle feed rate on holdup mass and heat transfer characteristics in cyclone heat exchanger. *Journal of Mechanical Science and Technology*, 29, 4509–4518. <https://doi.org/10.1007/s12206-015-0950-z>

Obermair, S., and Staudinger, G. (2001). The dust outlet of a gas cyclone and its effects on separation efficiency. *Chemical engineering & technology*, 24(12), 1259–1263. [https://doi.org/10.1002/1521-4125\(200112\)24](https://doi.org/10.1002/1521-4125(200112)24)

Obermair, S., Woisetschlager, J., and Staudinger, G. (2003). Investigation of the flow pattern in different dust outlet geometries of a gas cyclone by laser Doppler anemometry. *Powder Technology*, 138(2–3), 239–251. <https://doi.org/10.1016/j.powtec.2003.09.009>

Pouria, K. A. A., Javad V. N. N., Saeid K., and Danial K. A. A. (2023). A Dimensional optimization study on cyclone performance under the oscillating boundary condition. *Chemical Engineering and Processing - Process Intensification*, 183, 109217. <https://doi.org/10.1016/j.cep.2022.109217>.

Qian, F. P., Zhang, M. Y. (2005). Study of the natural vortex length of a cyclone with response surface methodology. *Computers & Chemical Engineering*, 29(10), 2155–2162. <https://doi.org/10.1016/j.compchemeng.2005.07.011>.

- Raoufi, A., Shams, M., and Kanani, H. (2009). CFD analysis of flow field in square cyclones. *Powder Technology*, 191(3), 349-357.
<https://doi.org/10.1016/j.powtec.2008.11.007>
- Ravi, S., Lakhbir, S. B. (2020). Numerical investigations of the flow-field inside cyclone separators with different cylinder-to-cone ratios using large-eddy simulation. *Separation and Purification Technology*, 249, 117149.
<https://doi.org/10.1016/j.seppur.2020.117149>
- Rietema, K., and Maatschappij, S. I. R. (1961). Performance and design of hydrocyclones—I: General considerations. *Chemical Engineering Science*, 15(3-4), 298-302.
[https://doi.org/10.1016/0009-2509\(61\)85033-1](https://doi.org/10.1016/0009-2509(61)85033-1)
- Shao, M. W. (1996). Analysis of the amplification effect of cyclone separators. *Ventilation and Dust Removal*. 04, 32-33.
- Shastri, R., Wasilewski, M., Lakhbir S. B. (2021). Analysis of the novel hybrid cyclone separators using large-eddy simulation. *Powder Technology*, 394, 951-969.
<https://doi.org/10.1016/j.powtec.2021.09.033>
- Shukla, S. K., Shukla, P., and Ghosh, P. (2013). The effect of modeling of velocity fluctuations on prediction of collection efficiency of cyclone separators. *Applied Mathematical Modelling*, 37(8), 5774-5789.
<https://doi.org/10.1016/j.apm.2012.11.019>
- Song, J. F., Wei, Y. D., Sun, G. G., Chen, J. Y. (2017). Experimental and CFD study of particle deposition on the outer surface of vortex finder of a cyclone separator. *Chemical Engineering Journal*, 309, 249-262.
<https://doi.org/10.1016/j.cej.2016.10.019>
- Sujeet, K. S., Shukla, P., Pradyumna, G. (2011). Evaluation of numerical schemes using different simulation methods for the continuous phase modeling of cyclone separators. *Advanced Powder Technology*, 22(02), 209-219.
<https://doi.org/10.1016/j.apt.2010.11.009>
- Sun, X. M., Zhang, Z. Z., Chen, D. R. (2017). Numerical modeling of miniature cyclone. *Powder Technology*, 320, 325-339.
<https://doi.org/10.1016/j.powtec.2017.07.053>
- Venkatesh, S., Sakthivel, M., Saranav, H., Saravanan, N., Rathnakumar, M., and Santhosh, K. K. (2020). Performance investigation of the combined series and parallel arrangement cyclone separator using experimental and CFD approach. *Powder Technology*, 361, 1070-1080.
<https://doi.org/10.1016/j.powtec.2019.10.087>
- Wang, C. W. (2020). A Study on the Characteristics and Mechanism of Short-circuit Flow in a Gas Cyclone. *Lanzhou University*
<https://doi.org/10.27204/d.cnki.glzhu.2020.000117>
- Wei, Q., Sun, G. G., Gao, C. Z. (2020). Numerical analysis of axial gas flow in cyclone separators with different vortex finder diameters and inlet dimensions. *Powder Technology*, 369, 321-333.
<https://doi.org/10.1016/j.powtec.2020.05.038>
- Yang, H. G., Wang, N., Cao, Y. X., Meng, X. J., Yao, L. (2023). Effects of helical fins on the performance of a cyclone separator: A numerical study. *Advanced Powder Technology*, 34(01), 103929.
<https://doi.org/10.1016/j.apt.2022.103929>
- Yuan, H. X., Li, L. L. (2010). Numerical simulation of the effect of physical and structural parameters on the pressure drop of cyclone separators. *Mining Machinery*, 38(05), 91-94.
<https://doi.org/10.16816/j.cnki.ksjx.2010.05.028>
- Yuan, Y., Sun G. G., Zhou, F. J., and Sun, Z. P. (2017). Effect of barrel diameter on cyclone performance. *Journal of Petroleum (Petroleum Processing)*, 34(04), 738-745.
- Zhang, G., Chen, G., Yan, X. H. (2018). Evaluation and improvement of particle collection efficiency and pressure drop of cyclones by redistribution of dustbins. *Chemical Engineering Research and Design*, 139, 52-61.
<https://doi.org/10.1016/j.cherd.2018.09.021>
- Zhang, T., Liu, C. J., Guo, K., Liu, H., and Wang, Z. C. (2016). Analysis of Flow Field in Optimal Cyclone Separators with Hexagonal Structure Using Mathematical Models and Computational Fluid Dynamics Simulation. *Industrial & Engineering Chemistry Research*, 55(01), 351-365.
<https://doi.org/10.1021/acs.iecr.5b02813>
- Zhang, Z. W., Li, Q., Zhang, Y. H., Wang, H. L. (2022). Simulation and experimental study of effect of vortex finder structural parameters on cyclone separator performance. *Separation and Purification Technology*, 286, 120394.
<https://doi.org/10.1016/j.seppur.2021.120394>
- Zhao, B. (2010). Development of a dimensionless logistic model for predicting cyclone separation efficiency. *Aerosol Science and Technology*, 44(12), 1105-1112.
<https://doi.org/10.1080/02786826.2010.512027>
- Zhao, B., Su, Y., Zhang, J. (2006). Simulation of Gas Flow Pattern and Separation Efficiency in Cyclone with Conventional Single and Spiral Double Inlet Configuration. *Chemical Engineering Research and Design*, 84(12), 1158-1165.
<https://doi.org/10.1205/cherd06040>
- Gao, X., Chen, J. F., Feng, J. M., Peng, X. Y. (2014). Numerical investigation of the effects of the central channel on the flow field in an oil-gas cyclone separator. *Computers & Fluids*, 92, 45-55.
<https://doi.org/10.1016/j.compfluid.2013.11.001>
- Li, X. D., Yan, J. H., Cao, Y. C., Ni, M. J., and Cen, K. F. (2003). Numerical simulation of the effects of turbulence intensity and boundary layer on separation efficiency in a cyclone separator. *Chemical Engineering Journal*, 95(1-3), 235-240.
[https://doi.org/10.1016/S1385-8947\(03\)00109-8](https://doi.org/10.1016/S1385-8947(03)00109-8)
- Farzad, P., Seyyed, H. H., Khairy, E., and Goodarz, A. (2018). Numerical investigation of effects of inner cone on flow field, performance and erosion rate of cyclone separators. *Separation and Purification Technology*, 201, 223-237.
<https://doi.org/10.1016/j.seppur.2018.03.001>